ARTICLE

Check for updates

Pseudospin-triplet pairing in iron-chalcogenide superconductors

Meng Zeng [1], Dong-Hui Xu[2,3], Zi-Ming Wang[2,3], Lun-Hui Hu [4,5✉] & Fu-Chun Zhang[6,7]

Understanding the pairing symmetry is a crucial theoretical aspect in the study of unconventional superconductivity for interpreting experimental results. Here we study superconductivity of electron systems with both spin and pseudospin-1/2 degrees of freedom. By solving linearized gap equations, we derive a weak coupling criterion for the even-parity spin-singlet pseudospin-triplet pairing. It can generally mix with the on-site s-wave pairing since both of them belong to the same symmetry representation (A_{1g}) and their mixture could naturally give rise to anisotropic intra-band pairing gap functions with or without nodes. This may directly explain why some of the iron-chalcogenide superconductors are fully gapped (e.g. FeSe thin film) and some have nodes (e.g. LaFePO and LiFeP). We also find that the anisotropy of gap functions can be enhanced when the principal rotation symmetry is spontaneously broken in the normal state such as nematicity, and the energetic stabilization of pseudospin-triplet pairings indicates the coexistence of nematicity and superconductivity. This could be potentially applied to bulk FeSe, where gap anisotropy has been experimentally observed.

[1] Department of Physics, University of California, San Diego, CA 92093, USA. [2] Department of Physics and Chongqing Key Laboratory for Strongly Coupled Physics, Chongqing University, Chongqing 400044, People's Republic of China. [3] Center of Quantum Materials and Devices, Chongqing University, Chongqing 400044, People's Republic of China. [4] Department of Physics, The Pennsylvania State University, University Park, PA 16802, USA. [5] Department of Physics and Astronomy, University of Tennessee, Knoxville, TN 37996, USA. [6] Kavli Institute for Theoretical Sciences, University of Chinese Academy of Sciences, 100190 Beijing, China. [7] CAS Center for Excellence in Topological Quantum Computation, University of Chinese Academy of Sciences, 100190 Beijing, China. ✉email: hu.lunhui.zju@gmail.com

The symmetry principle is one of the most powerful tools to diagnose low-energy electronic band structures, lattice vibrations, and linear responses[1], and is also valuable to explore various symmetry-breaking ordered phases such as magnetism, charge/spin density-wave, nematicity and superconductivity[2]. The crystal symmetry of a solid-state system dictates the normal band structures it hosts near the Fermi level, which could in turn determine the most favorable superconducting pairing symmetry[3,4]. This symmetry principle for superconductors (SC) is recently extended to investigate multi-band unconventional superconductivity[5–7]. Interestingly, the orbital-independent and orbital-dependent pairings that belong to the same symmetry representation may coexist with each other[8]. Such orbital-dependent pairings have been studied in a wide variety of systems with multi-band character, including Sr_2RuO_4[9], iron-chalcogenide SCs[10–13], Cu-doped Bi_2Se_3[14] and half-Heusler compounds[15–18], from which the guiding principle by symmetry is crucial to understanding the nature of unconventional superconductivity.

A few specific systems can be effectively characterized by a general normal-state model Hamiltonian that contains both spin ($\{\uparrow, \downarrow\}$) and pseudospin ($\{1, 2\}$) degrees of freedom, where pseudospin could originate from two atomic orbitals, two sublattices, two layers, or two valleys[6]. We start from a spin-singlet centrosymmetric SC to explore the existence of even-parity pseudospin-triplet pairings, for example, $c_{1,\uparrow}(\mathbf{k})c_{2,\downarrow}(-\mathbf{k}) + c_{2,\uparrow}(\mathbf{k})c_{1,\downarrow}(-\mathbf{k}) - c_{1,\downarrow}(\mathbf{k})c_{2,\uparrow}(-\mathbf{k}) - c_{2,\downarrow}(\mathbf{k})c_{1,\uparrow}(-\mathbf{k})$, and further investigate their valuable roles in tailoring anisotropic pairing gap functions with or without nodes[19]. Different from spin-triplet pairings, spin-singlet pseudospin-triplet pairings have not been much explored in real materials since such pairings are usually considered to be energetically unfavorable. This is partly due to the common belief that the double degeneracy of the two orbitals is lifted by orbital hybridization so that the orbital-dependent pairing would be severely suppressed under crystal field splitting or electron-electron repulsive interaction. One aim of this work is concerned with the possible condition for the existence of even-parity spin-singlet orbital-dependent pairings, and possible applications to real materials.

On the other hand, the effects of symmetry breaking in unconventional SCs is an important topic that has attracted tremendous interest. The symmetry could be broken explicitly by external fields or strain, or be broken spontaneously from many-body interactions. Two typical examples are rotational symmetry breaking[20,21] and time-reversal-symmetry (TRS) breaking[22–26]. Besides, the interplay between nematicity and superconductivity is yet to be fully understood in some real materials, such as FeSe[12,27], where gap functions can be highly anisotropic. These systems are all multi-band SCs, while symmetry-reducing signatures are experimentally observed above the superconducting transition temperature, which is mainly caused by both crystal field splittings and interaction-induced order parameters (e.g. nematicity). Thus, discovering the coexistence of nematicity and superconductivity in these multi-band systems can shed new light on understanding the underlying favorable pairing symmetries.

The main finding of this work is that the anisotropic gap functions with or without nodes could be attributed to the mixing of isotropic s-wave pairing and even-parity spin-singlet pseudospin-triplet pairing, even though both of them belong to the A_{1g} symmetry representation. For technical conveniences, we adopt an orbital $\mathbf{d}_o(\mathbf{k})$-vector notations[11] to describe the pairing matrix and similarly a $\mathbf{g}_o(\mathbf{k})$-vector for orbital hybridization in the two-orbital subspace ($\{1, 2\}$). Solving linearized gap equations, we show that the presence of $\mathbf{g}_o$-vector generally suppresses the superconductivity with orbital $\mathbf{d}_o$-vector except for $\mathbf{d}_o(\mathbf{k}) \| \mathbf{g}_o(\mathbf{k})$, which is consistent with the concept of superconducting fitness[6].

This sets up weak-coupling criteria for A_{1g}-type orbital-dependent pairings that could naturally give rise to anisotropic gap functions in real superconducting materials. Moreover, we reveal a deep connection between two-orbital nematic SC and pseudospin-triplet pairings. Within the mean-field theory for electron-electron repulsive interactions, the nematic order develops in the orbital subspace at $T < T_{nem}$, which also contributes to the total orbital hybridization, $\mathbf{g}_{tot} = \mathbf{g}_o + \mathbf{g}_{nem}$. This leads to the stabilization of a nematic orbital $\mathbf{d}_o$-vector for $\mathbf{d}_o(\mathbf{k}) \| \mathbf{g}_{tot}(\mathbf{k})$, indicating the coexistence of nematicity and superconductivity. The direct applications to FeSe[12,27] are also discussed. We also generalize it to a two-valley system with C_6 breaking terms (e.g., Kekulé distortion). In the end, we also predict an orbital-polarized superconducting state.

Results

Classification of Spin-singlet Orbital-triplet pairings. To explore the weak-coupling criterion for the energetically favorable even-parity spin-singlet pseudospin-triplet pairing, we consider the mean-field pairing Hamiltonian,

$$\mathcal{H}_\Delta = \sum_{\mathbf{k}} \sum_{s_1 a, s_2 b} \Delta^{a,b}_{s_1, s_2}(\mathbf{k}) F^\dagger_{s_1 a, s_2 b}(\mathbf{k}) + \text{h.c.}, \quad (1)$$

where $F^\dagger_{s_1 a, s_2 b}(\mathbf{k}) = c^\dagger_{s_1 a}(\mathbf{k}) c^\dagger_{s_2 b}(-\mathbf{k})$ is the creation operator of Cooper pairs, s_1, s_2 are indices for spins and a, b are for pseudospins (e.g., two orbitals $\{1, 2\}$). A general pairing potential of a two-band model is a four-by-four matrix[6]. In particular, the spin-singlet pairing function $\Delta^{a,b}_{s_1, s_2}(\mathbf{k}) = f(\mathbf{k}) M_{a,b}(\mathbf{k})(i\sigma_2)_{s_1, s_2}$ consists of the angular form factor $f(\mathbf{k})$ and $M_{a,b}(\mathbf{k})$ in the orbital channel. The spin-singlet pairings are not mixed with spin-triplet pairings in the absence of spin-orbit coupling (SOC). In analogy to spin-triplet SCs, for the technical convenience, we then use an orbital $\mathbf{d}_o(\mathbf{k})$-vector for the spin-singlet orbital-dependent pairing potential[11],

$$\hat{\Delta}_{tot}(\mathbf{k}) = [\Delta_s \Psi_s(\mathbf{k}) \tau_0 + \Delta_o (\mathbf{d}_o(\mathbf{k}) \cdot \boldsymbol{\tau})](i\sigma_2), \quad (2)$$

where Δ_s and Δ_o are pairing strengths in orbital-independent and orbital-dependent channels, respectively. Here $\boldsymbol{\tau}$ and $\boldsymbol{\sigma}$ are Pauli matrices acting on the orbital and spin subspace, respectively, and τ_0 is a 2-by-2 identity matrix. When both Δ_s and Δ_o are real, a real orbital $\mathbf{d}_o(\mathbf{k})$-vector preserves TRS while a complex one spontaneously breaks TRS ($\mathcal{T} = i\tau_0\sigma_2\mathcal{K}$ with $\mathcal{K}$ being complex conjugate). The Fermi statistics requires $\Psi_s(\mathbf{k}) = \Psi_s(-\mathbf{k})$, $d^{1,3}_o(\mathbf{k}) = d^{1,3}_o(-\mathbf{k})$ and $d^2_o(\mathbf{k}) = -d^2_o(-\mathbf{k})$. In other words, $d^2_o(\mathbf{k})$ describes odd-parity spin-singlet orbital-singlet pairings and the other two are for even-parity spin-singlet orbital-triplet pairings. Moreover, we provide an alternative definition of orbital $\mathbf{d}_o$-vectors in Supplementary Note 1. Even though the orbital-independent part $\Psi_s(\mathbf{k})$ is also "orbital-triplet" by statistics, it is completely trivial. Hereafter, we only refer to $d^1_o(\mathbf{k})$ and $d^3_o(\mathbf{k})$ as orbital-triplet pairings[28].

In addition, the basis functions for both $\Psi_s(\mathbf{k})$ and orbital $\mathbf{d}_o(\mathbf{k})$-vectors in Eq. (2) could be classified by crystalline symmetry.

Under the action of an n-fold rotation operator C_n about the z-axis, the pairing potential $\hat{\Delta}(\mathbf{k})$ transforms as

$$\mathcal{D}[C_n] \hat{\Delta}_J(\mathbf{k}) (\mathcal{D}[C_n])^T = e^{i\frac{2\pi}{n}J} \hat{\Delta}_J(C_n^{-1}\mathbf{k}), \quad (3)$$

where $\mathcal{D}[C_n]$ is the corresponding matrix representation, J is the orbital angular momentum quantum number, and also labels the irreducible representations of the C_n point group. For example, $J = 0$ is for A representation and $J = 2$ is for B representation. Firstly, the TRS requires the coexistence of $\hat{\Delta}_J$ and $\hat{\Delta}_{-J}$ with equal weight. If the rotation symmetry C_n is further imposed, then J

Table 1 Classification of spin-singlet pairing potentials for Eq. (2).

C_n	$J = -J \pmod{n}$	$\Psi_s(\mathbf{k}) = \Psi_s(-\mathbf{k})$	$\mathbf{d}_o^1(\mathbf{k}) = \mathbf{d}_o^1(-\mathbf{k})$	$\mathbf{d}_o^2(\mathbf{k}) = -\mathbf{d}_o^2(-\mathbf{k})$	$\mathbf{d}_o^3(\mathbf{k}) = \mathbf{d}_o^3(-\mathbf{k})$
$n = 2$	$J = 0$	$1, k_x^2, k_y^2, k_z^2, k_x k_y$	$1, k_x^2, k_y^2, k_z^2, k_x k_y$	$k_z, k_z k_x^2, k_z k_y^2, k_z^3, k_z k_x k_y$	$1, k_x^2, k_y^2, k_z^2, k_x k_y$
	$J = 1$	$k_x k_z, k_y k_z$	$k_x k_z, k_y k_z$	k_x, k_y	$k_x k_z, k_y k_z$
$n = 3$	$J = 0$	$1, k_x^2 + k_y^2, k_z^2$	E_g representation	k_z	E_g representation
$n = 4$	$J = 0$	$1, k_x^2 + k_y^2, k_z^2$	$k_x^2 - k_y^2, k_x k_y$	$k_z, k_z(k_x^2 + k_y^2), k_z^3$	$k_x^2 - k_y^2, k_x k_y$
	$J = 2$	$k_x^2 - k_y^2, k_x k_y$	$1, k_x^2 + k_y^2, k_z^2$	$k_z(k_x^2 - k_y^2), k_z k_x k_y$	$1, k_x^2 + k_y^2, k_z^2$
$n = 6$	$J = 0$	$1, k_x^2 + k_y^2, k_z^2$	E_g representation	k_z	E_g representation
	$J = 3$	$(k_x + ik_y)^3, (k_x - ik_y)^3$	E_g representation	$k_x^3 - 3k_x k_y^2, 3k_x^2 k_y - k_y^3$	E_g representation

Here we consider a spin-singlet two-orbital superconductors with $\{d_{xz}, d_{yz}\}$-orbitals. Based on the n-fold rotation symmetry C_n about z-axisd and time-reversal symmetry (TRS), we have $J = -J$ mod n, which leads to all the pairing channels with orbital-independent $\Psi_s(\mathbf{k})$ and orbital-dependent $\mathbf{d}_o(\mathbf{k})$-vector in Eq. (2). Here, for $J = 0$ pairing subspace of C_3, the $(\mathbf{d}_o^1(\mathbf{k}), \mathbf{d}_o^3(\mathbf{k}))$ forms a two-dimensional E_g representation, where the basis functions are $(k_x^2 - k_y^2, k_x k_y)$ and $(k_y k_z, k_x k_z)$. For $J = 0$ pairing subspace of C_6, the $(\mathbf{d}_o^1(\mathbf{k}), \mathbf{d}_o^3(\mathbf{k}))$ forms a two-dimensional E_g representation, where the basis functions are $(k_y k_z, k_x k_z)$; for the $J = 3$ pairing subspace of C_6, the $(\mathbf{d}_o^1(\mathbf{k}), \mathbf{d}_o^3(\mathbf{k}))$ forms a two-dimensional E_g representation, where the basis functions are $(k_x^2 - k_y^2, k_x k_y)$.

and $-J$ have to be equivalent modulo n, i.e. $J \equiv -J$ mod n. The results for the basis functions of $\Psi_s(\mathbf{k})$ and $\mathbf{d}_o(\mathbf{k})$ are summarized in Table 1 for a two-band SC with the $\{d_{xz}, d_{yz}\}$-orbitals. In this case, $\mathcal{D}[C_n] = [\cos(\frac{2\pi}{n})\tau_0 - i\sin(\frac{2\pi}{n})\tau_2] \otimes \sigma_0$. For instance, $\mathcal{D}[C_4] = -i\tau_2 \otimes \sigma_0$ explains that both $\Delta_o \tau_1$ and $\Delta_o \tau_3$ are d-wave-like pairing states[29].

At the mean-field level, the Bogoliubov de-Gennes (BdG) Hamiltonian is given by

$$\mathcal{H}_{\mathrm{BdG}} = \begin{pmatrix} \mathcal{H}_0(\mathbf{k}) & \hat{\Delta}_{tot}(\mathbf{k}) \\ \hat{\Delta}_{tot}^\dagger(\mathbf{k}) & -\mathcal{H}_0^*(-\mathbf{k}) \end{pmatrix}, \tag{4}$$

where $\mathcal{H}_0(\mathbf{k})$ represents a two-band normal-state Hamiltonian with both spin and pseudospin degrees of freedom.

In general, the BdG Hamiltonian is also invariant under the C_n rotation symmetry, i.e., $\mathcal{D}_{\mathrm{BdG}}[C_n] \mathcal{H}_{\mathrm{BdG}}(\mathbf{k}) (\mathcal{D}_{\mathrm{BdG}}[C_n])^\dagger = \mathcal{H}_{\mathrm{BdG}}(C_n^{-1}\mathbf{k})$ when we define $\mathcal{D}_{\mathrm{BdG}}[C_n] = \begin{pmatrix} \mathcal{D}[C_n] & 0 \\ 0 & e^{i\frac{2\pi}{n}J}(\mathcal{D}[C_n])^* \end{pmatrix}$ based on Eq. (3).

Here we assume both inversion and time-reversal symmetries are preserved. To be specific, we consider a SOC-free Hamiltonian,

$$\mathcal{H}_0(\mathbf{k}) = \epsilon(\mathbf{k})\tau_0 \sigma_0 + \lambda_o(\mathbf{g}_o(\mathbf{k}) \cdot \boldsymbol{\tau})\sigma_0, \tag{5}$$

where the basis is $\psi_\mathbf{k}^\dagger = (c_{1,\uparrow}^\dagger(\mathbf{k}), c_{1,\downarrow}^\dagger(\mathbf{k}), c_{2,\uparrow}^\dagger(\mathbf{k}), c_{2,\downarrow}^\dagger(\mathbf{k}))$, $\epsilon(\mathbf{k}) = (k_x^2 + k_y^2)/2m - \mu$ is the band energy measured relative to the chemical potential μ, m is the effective mass, λ_o represents the orbital hybridization and $\mathbf{g}_o(\mathbf{k}) = (g_1(\mathbf{k}), g_2(\mathbf{k}), g_3(\mathbf{k}))$. And the g_3-component leads to the different effective masses of different orbitals. As mentioned earlier, this vector notation is just for the technical convenience. Besides, the g_1 and g_2 components are determined by symmetries. For example, TRS requires $g_{1,3}(\mathbf{k}) = g_{1,3}(-\mathbf{k})$ and $g_2(\mathbf{k}) = -g_2(-\mathbf{k})$. If inversion symmetry (IS) is present, $g_2(\mathbf{k})$ (or $g_1(\mathbf{k})$) must vanish for $\mathcal{I} = \tau_0 \sigma_0$ (or $\mathcal{I} = \tau_3 \sigma_0$), which is the same as the constraint for the orbital $\mathbf{d}_o(\mathbf{k})$-vector. The more explicit form of $\mathbf{g}_o(\mathbf{k})$ is determined by other crystal symmetries.

In general, the pseudospin-triplet (i.e. orbital-triplet) pairing state shares some similarities with the spin-triplet pairing state[30]. To show that, we first discuss the superconducting quasi-particle spectrum of orbital-triplet SCs in the absence of band-splitting caused by orbital hybridizations, i.e., $\mathbf{g}_o(\mathbf{k}) = 0$ for Eq. (5). In this case, the superconducting gaps on the Fermi surface are

$$E(\mathbf{k}) = \pm |\Delta_o| \sqrt{|\mathbf{d}_o(\mathbf{k})|^2 \pm |\mathbf{d}_o^*(\mathbf{k}) \times \mathbf{d}_o(\mathbf{k})|}, \tag{6}$$

for the $\Delta_s = 0$ limit. This indicates that there are two distinct gaps

if TRS is spontaneously broken. In the following, we mainly focus on the time-reversal-invariant superconducting states, i.e., real $\mathbf{d}_o$-vectors, for which the classification of pairing potentials is shown in Table 1 based on Eq. (3). We will show the interplay between Δ_s and Δ_o can lead to anisotropic superconducting gaps on different Fermi surfaces. Moreover, its stability against orbital-hybridization, electron-electron interactions, and applications to real materials will be discussed in detail as follows. We will also briefly comment on the effects of TRS-breaking in the end.

Stability for spin-singlet orbital-triplet pairings. We apply the weak-coupling scheme[6] for spin-singlet orbital-triplet pairings against crystal field splittings, which cause orbital hybridizations [i.e. the $\mathbf{g}_o(\mathbf{k})$ term in Eq. (5)]. We analytically calculate the superconductivity instability for the orbital $\mathbf{d}_o$-vector by BCS decoupling scheme. The superconducting transition temperature T_c of orbital-dependent pairing channels is calculated by solving the linearized gap equation,

$$\Delta_{s_1, s_2}^{a, b}(\mathbf{k}) = -\frac{1}{\beta} \sum_{\omega_n} \sum_{s_1' a', s_2' b'} V_{s_1' a', s_2' b'}^{s_1 a, s_2 b}(\mathbf{k}, \mathbf{k}')$$
$$\times \left[G_e(\mathbf{k}', i\omega_n) \hat{\Delta}(\mathbf{k}') G_h(-\mathbf{k}', i\omega_n) \right]_{s_1' a', s_2' b'}, \tag{7}$$

where $\beta = 1/k_B T$, $G_e(\mathbf{k}, i\omega_n) = [i\omega_n - \mathcal{H}_0(\mathbf{k})]^{-1}$ is the Matsubara Green's function for electrons with $\omega_n = (2n + 1)\pi/\beta$ and $G_h(\mathbf{k}, i\omega_n) = -G_e^*(\mathbf{k}, i\omega_n)$. We expand the attractive interactions as $V_{s_1' a', s_2' b'}^{s_1 a, s_2 b}(\mathbf{k}, \mathbf{k}') = -\sum_{\Gamma, l} [v^\Gamma \mathbf{d}_o^{\Gamma, l}(\mathbf{k}) \cdot \boldsymbol{\tau} i\sigma_2]_{s_1 a, s_2 b} [\mathbf{d}_o^{\Gamma, l}(\mathbf{k}') \cdot \boldsymbol{\tau} i\sigma_2]_{s_1' a', s_2' b'}$ with $v^\Gamma > 0$. Here Γ labels the irreducible representation with $l = 1, 2, ..., \mathrm{Dim}\,\Gamma$. In this work we focus on 1d representations, i.e. $\mathrm{Dim}\,\Gamma = 1$, which already include many interesting cases and are sufficient for the applications discussed in later sections. Due to the possible existence of multiple pairing channels belonging to different representations, each channel has its own critical temperature T_c^Γ, the largest of which becomes the actual critical temperature of the system. In the weak-coupling theory, T_c^Γ follows the standard BCS form and is solely determined by the corresponding pairing interaction v^Γ in that particular channel. To the leading order of $\lambda_o k_F^2/\mu$ ($k_F = \sqrt{2m\mu}$), the equation for T_c for the channel Γ reads (see details in the Methods section),
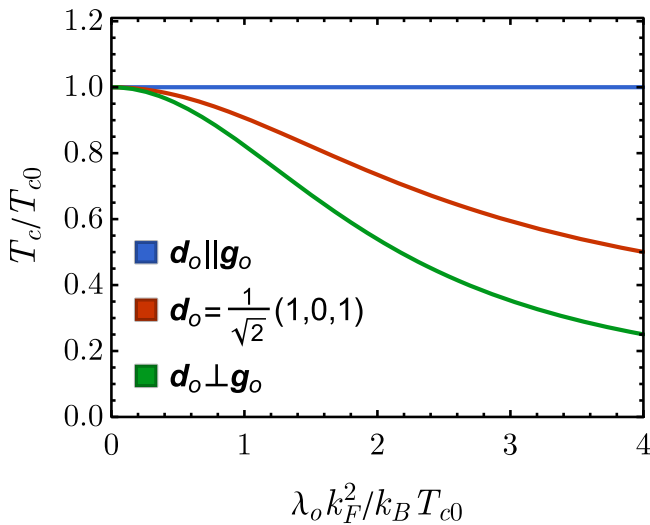
$$\ln\left(\frac{T_c^\Gamma}{T_{c0}}\right) = \int_S d\Omega\, \mathcal{C}_0(T_c)\left(\left|\mathbf{d}_o^\Gamma\right|^2 - \left|\mathbf{d}_o^\Gamma \cdot \hat{\mathbf{g}}_o\right|^2\right), \tag{8}$$

where T_{c0} is the critical temperature for $\lambda_o = 0$, Ω is the solid angle of $\mathbf{k}$, $\hat{\mathbf{g}}_o = \mathbf{g}_o(\mathbf{k})/|\mathbf{g}_o(\mathbf{k})|$ are normalized vectors. Here we take $\int_S d\Omega\, |\mathbf{d}_o^\Gamma|^2 = 1$. And $\mathcal{C}_0(T_c) = \mathrm{Re}\,[\psi^{(0)}(\frac{1}{2}) - \psi^{(0)}(\frac{1}{2} + i\frac{\lambda_o |\mathbf{g}(\mathbf{k})|}{2\pi k_B T_c})]$, where $\psi^{(0)}(z)$ is the digamma function.

We now discuss its implications. In general, the λ_o-term describes a pair-breaking term, since $\mathcal{C}_0(T_c) \leq 0$ and it monotonically decreases as λ_o increases, hence the right-hand side of Eq. (8) suppresses T_c in general. However, if we focus on one-dimensional representations, i.e. Dim $\Gamma = 1$, it is straightforward to see that $\mathbf{d}_o^\Gamma \parallel \mathbf{g}_o$ can lead to $T_c = T_{c0}$ for any value of λ_o, which indicates that the orbital $\mathbf{d}_o$-vector that is parallel with $\mathbf{g}_o$ is unaffected by the orbital hybridizations. It is worth mentioning that due to the possible suppression of T_c, depending on the relation between $\mathbf{d}_o^\Gamma$ and $\mathbf{g}_o$ the leading instability channel at $\lambda_o = 0$ could be suppressed more than some of the other coexisting channels and may eventually become sub-leading. This interesting behavior is discussed further in Supplementary Note 3. For notional simplicity, we will drop the representation index Γ when there is no danger of confusion. Choosing $\mathbf{g}_o(\mathbf{k}) = (2k_xk_y, 0, k_x^2 - k_y^2)$, the numerical results are shown in Fig. 1. The black line confirms that T_c is unaffected as $\lambda_o k_F^2/k_B T_{c0}$ increases for $\mathbf{d}_o(\mathbf{k}) = k_F^{-2}(2k_xk_y, 0, k_x^2 - k_y^2)$, which is the unconventional A_{1g} pairing. However, T_c for other $\mathbf{d}_o$-vectors are severely suppressed. The light-blue line is for $\mathbf{d}_o(\mathbf{k}) = \frac{1}{\sqrt{2}}(1, 0, 1)$, and the light-orange line for $\mathbf{d}_o(\mathbf{k}) = k_F^{-2}(k_x^2 - k_y^2, 0, -2k_xk_y)$. Therefore, we conclude that the orbital $\mathbf{d}_o$-vector could exist in SCs with two active orbitals that are not fully degenerate. This is similar to spin-triplet SCs, where the A_{1g}-type spin $\mathbf{d}_s$-vector could exist in noncentrosymmetric SCs because $\mathbf{d}_s \parallel \mathbf{g}_s$ is optimally satisfied[4,6].

It is worth mentioning that the results presented above is using a continuum form of the Hamiltonian based on $\mathbf{k} \cdot \mathbf{p}$ theory. For real materials, given the interaction on the lattice, the components of the interaction in terms of the basis functions of the representations might not be exactly the same with the form of the vector $\mathbf{g}_o$. As a result, the parallel condition presented above may not exactly satisfied. However, the theory developed in this work is generally applicable and the extend to which the parallel condition holds can still be a useful criterion for the most favorable pairing.

Next, we include Δ_s, and investigate the coupling between Ψ_s and $\mathbf{d}_o$. Solving the coupled linearized gap equations up to

$(\lambda_o k_F^2/\mu)^2$ order (see details in Supplementary Note 3), we find that the results from Eq. (8) are still correct. Besides, the magnitude of orbital $\mathbf{d}_o$-vectors might be determined as $\mathbf{d}_o(\mathbf{k}) = \Psi_s(\mathbf{k})\hat{\mathbf{g}}_o(\mathbf{k})$. It implies that Ψ_s and $\mathbf{d}_o$ belong to the same representation of crystalline groups. Therefore, the stability of orbital $\mathbf{d}_o$-vector by Eq. (8) indicates the symmetry principle for spin-singlet orbital-triplet pairings.

We now explain Eq. (8) from the band picture. Within the band basis, the pairing potential in the orbital subspace becomes $\hat{\Delta}_{\mathrm{band}}(\mathbf{k}) = U^\dagger(\mathbf{k})[\Delta_s\Psi_s(\mathbf{k})\tau_0 + \Delta_o(\mathbf{d}_o(\mathbf{k}) \cdot \boldsymbol{\tau})]U(\mathbf{k})$, where $U(\mathbf{k})$ is the unitary matrix in the orbital subspace, $U^\dagger(\mathbf{k})[\epsilon(\mathbf{k})\tau_0 + \lambda_o(\mathbf{g}_o(\mathbf{k}) \cdot \boldsymbol{\tau})]U(\mathbf{k}) = \mathrm{Diag}[E_+(\mathbf{k}), E_-(\mathbf{k})]$, with the normal band dispersion

$$E_\pm(\mathbf{k}) = \epsilon(\mathbf{k}) \pm \lambda_o|\mathbf{g}_o(\mathbf{k})|. \qquad (9)$$

The intra-orbital pairing naturally gives rise to the intra-band pairing. However, it is different for orbital-dependent pairings. To show that, we decompose the orbital $\mathbf{d}_o$-vector, $\mathbf{d}_o(\mathbf{k}) = d_\parallel(\mathbf{k})\hat{\mathbf{g}}_o(\mathbf{k}) + \mathbf{d}_\perp(\mathbf{k})$, where $d_\parallel(\mathbf{k}) = \mathbf{d}_o(\mathbf{k}) \cdot \hat{\mathbf{g}}_o(\mathbf{k})$ and $\mathbf{d}_\perp(\mathbf{k}) \cdot \hat{\mathbf{g}}_o(\mathbf{k}) = 0$. We find that the $d_\parallel$-part gives rise to the intra-band pairing, while the $\mathbf{d}_\perp$-part leads to the inter-band pairing (see Supplementary Note 4). If the band splitting is much larger than the pairing gap ($\lambda_o k_F^2 \gg \Delta_o$), the inter-band pairing is not energetically favorable in the weak-coupling pairing limit. It means that the inter-band pairing will be severely suppressed if we increase the orbital hybridization λ_o, consistent with Eq. (8) and results in Fig. 1. Now if we again include the orbital-independent pairing part $\Delta_s\Psi_s(\mathbf{k}\tau_0 i\sigma_2)$, the relation between $\mathbf{d}_o$ and $\Psi_s(\mathbf{k})$ obtained previously from solving the coupled linearized gap equation (see Supplementary Note 3) can also be reproduced in the band picture by considering the maximization of the condensation energy. The total condensation energy per volume and per spin of the two intra-band pairings is given by

$$
\begin{aligned}
\delta E = &N_+ \sum_{\mathbf{k} \in \mathrm{FS}_+} \left(\Delta_s\Psi_s(\mathbf{k}) + \Delta_o d_\parallel(\mathbf{k})\right)^2 \\
&+ N_- \sum_{\mathbf{k} \in \mathrm{FS}_-} \left(\Delta_s\Psi_s(\mathbf{k}) - \Delta_o d_\parallel(\mathbf{k})\right)^2,
\end{aligned} \qquad (10)
$$

where $N_\pm$ are the density of states on the two Fermi surfaces ($E_\pm$). And $\Delta_s\Psi_s(\mathbf{k}) \pm \Delta_o d_\parallel(\mathbf{k})$ are the pairing gaps on these two Fermi surfaces. In order to maximize δE, we have $d_\parallel(\mathbf{k}) = \mathrm{sign}[(N_+ - N_-)\Delta_s\Delta_o]\Psi_s(\mathbf{k})$ (See Supplementary Note 4 for details). Even though the intra-orbital pairing and the orbital-triplet pairing belong to the same symmetry representation, the different $\mathbf{k}$-dependencies of $\Psi_s(\mathbf{k})$ and $d_\parallel(\mathbf{k})$ can naturally lead to the anisotropic superconducting gap on the Fermi surface observed in experiments.

Applications to superconductors with/without nodes. As a consequence of the mixing of the orbital-independent pairing (Δ_s) and orbital-dependent pairing (Δ_o) discussed in the previous section, there could be a nodal SC. In this section, we apply the results of the previous section to study superconductors with two orbitals, where Δ_s and Δ_o coexist. It is shown that the anisotropic gap functions with/without nodes depend on the ratio of Δ_s and Δ_o superconducting order parameters. Our weak-coupling theory might have potential applications to some of the nodal/nodeless SCs in the iron-chalcogenides family. For example, the angle-resolved photoemission spectroscopy (ARPES) measurements indicate a nontrivial superconducting gap anisotropy for the monolayer FeSe thin film[31]. The penetration depth measurements on both LaFePO[32] and LiFeP[33] show a linear dependence on T, suggesting the presence of superconducting gap nodes.

Fig. 1 Stability of orbital $\mathbf{d}_o$-vectors vs orbital hybridization λ_o in Eq. (5). It shows the transition temperature T_c/T_{c0} as a function of $\lambda_o k_F^2/k_B T_{c0}$ for $\mathbf{g}_o(\mathbf{k}) = (2k_xk_y, 0, k_x^2 - k_y^2)$. T_{c0} is T_c at $\lambda_o = 0$. The curves from top to bottom correspond to $\mathbf{d}_o(\mathbf{k}) = k_F^{-2}(2k_xk_y, 0, k_x^2 - k_y^2)$, $\mathbf{d}_o(\mathbf{k}) = \frac{1}{\sqrt{2}}(1, 0, 1)$, and $\mathbf{d}_o(\mathbf{k}) = k_F^{-2}(k_x^2 - k_y^2, 0, -2k_xk_y)$, respectively.

As an example, we consider the pairing potential in Eq. (2) for monolayer FeSe, where there is no hole pocket around the Γ-point, and a two-spin two-orbital model has been shown to be a good approximation around the electron pockets near the M point of the Brillouin zone (two Fe unit cell). The density functional theory calculations show that there are four bands around the M point, giving rise to only two electron pockets. In the one Fe unit cell, there is one pocket near the X and Y points, respectively. After folding with respect to the unit cell with two Fe, we obtain two pockets around the M point. Considering spin degrees of freedom, it naturally resembles a C_{4z}-invariant two-orbital model[34],

$$\mathcal{H}_M(\mathbf{k}) = \left[\epsilon(\mathbf{k})\tau_0 + Ak_x k_y \tau_z\right]\sigma_0 + v_{so}\tau_x\left[k_x\sigma_y + k_y\sigma_x\right], \quad (11)$$

where $\epsilon(\mathbf{k}) = (k_x^2 + k_y^2)/(2m) - \mu$ with $m > 0$ the effective mass, A leads to the anisotropic effective mass (i.e., orbital hybridization), and v_{so} represents SOC that still preserves inversion symmetry. These four states are degenerate at the M point since they form the four-dimensional representation of the space group No. 129 ($P4/nmm$)[35]. We take the parameters for the FeSe thin film as $\mu = 55$ meV, $1/(2m) = 1375$ meV $\cdot$ Å^2, $A = 600$ meV $\cdot$ Å^2 and $v_{so} \leq 15$ meV $\cdot$ Å[34]. The SOC is very weak to open a tiny gap along the $k_x = 0$ and $k_y = 0$ lines, shown in Fig. 2a. As what we expect, it shows two C_{4z} rotational-invariant Fermi surfaces, and the maximal gap, which is induced by the z-component of the $\mathbf{g}_o$ vector, is around 12 meV along the (11) and (1$\bar{1}$) directions. This is larger than the typical superconducting gaps in iron-chalcogenide SCs (~4 meV), implying that the effect of the orbital hybridization on the pairing symmetries should not be neglected.

We now use the criteria derived above (Eq. (8)) to examine the superconducting states. Specifically, the weak-coupling criterion indicates that the most favorable pairing to characterize the anisotropic superconducting gap is the A_{1g}-type s-wave pairing symmetry,

$$\hat{\Delta}(\mathbf{k}) = \left[\Delta_s\tau_0 + \Delta_o k_x k_y \tau_z\right](i\sigma_2). \quad (12)$$

The ratio between Δ_s and Δ_o determines the superconducting nodal structure. To simplify the analysis, we turn off the weak SOC. In the band basis, the dispersion of $\mathcal{H}_M(\mathbf{k})$ is $\epsilon_\pm(\mathbf{k}) = (k_x^2 + k_y^2)/(2m) \pm A|k_x k_y| - \mu$. Here $\pm$ label the band index. Projecting $\hat{\Delta}(\mathbf{k})$ onto the bands leads to $\Delta_\pm = \Delta_s \pm \Delta_o|k_x k_y|$. Given that $\Delta_s, \Delta_o > 0$, nodal points can only appear for Δ_- on the "$-$" band. The nodal condition would be $|k_x k_y| = \Delta_s/\Delta_o$ has solution on the FS given by $\epsilon_-(\mathbf{k}) = 0$. By using the mathematical inequality $k_x^2 + k_y^2 \leq 2|k_x k_y|$, it can be shown that the nodal

condition is given by,

$$\frac{\Delta_s}{\Delta_o} \leq \frac{\mu}{1/m - A}, \quad (13)$$

which is shown in Fig. 2b. In general, the ratio Δ_s/Δ_o should depend on both interaction strength in each pairing channel and the orbital hybridization strength. This gives rise to the condition of nodal A_{1g}-type s-wave superconducting states. Therefore, it could not only explain the anisotropic gap functions observed in the FeSe thin film (fully gapped) but also the nodal superconductivity in LaFePO and LiFeP. Around one linear Dirac node, the effective Hamiltonian up to linear-k can be mapped out as

$$\mathcal{H}_D = k_1\tilde{\sigma}_0\tilde{\tau}_z + k_2\tilde{\sigma}_y\tilde{\tau}_y, \quad (14)$$

where k_1, k_2 are liner combinations of k_x and k_y. All the other Dirac nodes are related to this one by reflection symmetries. Then, we only need to focus on $\mathcal{H}_D$, which is a Dirac Hamiltonian with topological charge (winding number) ± 2, whose node is protected by the chiral symmetry (i.e., the product of time-reversal symmetry and particle-hole symmetry). The $2\mathbb{Z}$ winding number is due to the presence of inversion symmetry and time-reversal symmetry. To analytically show the topology of Dirac nodes, we apply perturbation analysis with respect to PT symmetry (i.e., the product of time-reversal symmetry and inversion symmetry) and Chiral symmetry. Note that the PT symmetry can be also $C_{2z}T$ symmetry for a 2D or quasi-2D SC. The projected symmetry representations are given by PT $= \tilde{\sigma}_y\tilde{\tau}_0$ and $\mathcal{C} = \tilde{\sigma}_y\tilde{\tau}_x$. As expected, the PT symmetry commutes with $\mathcal{H}_D$, while the Chiral symmetry anti-commutes with $\mathcal{H}_D$. Then, local perturbations preserving PT and Chiral are

$$\mathcal{H}_D' = m_1\tilde{\sigma}_0\tilde{\tau}_y + m_2\tilde{\sigma}_y\tilde{\tau}_z, \quad (15)$$

where m_1 and m_2 represent perturbation strengths or mass terms. The spectrum of $\mathcal{H}_D + \mathcal{H}_D'$ are given by

$$E = \pm\sqrt{k_1^2 + k_2^2 + m_1^2 + m_2^2 \pm 2|m_1 k_2 + m_2 k_1|}, \quad (16)$$

which indicates that the Dirac nodes are movable but not removable. For example, $k_1 = 510.7k_x + 76.5k_y$ and $k_2 = -14.7k_x - 40.9k_y$ around one Dirac node. Then, turning on the SOC $v_{so} = 15$ meV $\cdot$ Å, we numerically confirm the nodal SC phase with $\Delta_s = 3$ meV and $\Delta_o = 200$ meV $\cdot$ Å^2, shown in Fig. 2c, where the logarithm of superconducting gaps are plotted. The eight dark red points are the linear Dirac nodes. Based on the topology-protection argument, the interplay between intra- and inter-orbital pairings for nodal superconductivity is robust against local perturbations. Note that our results are different from a previous work[34], in which the d-wave pairing symmetry
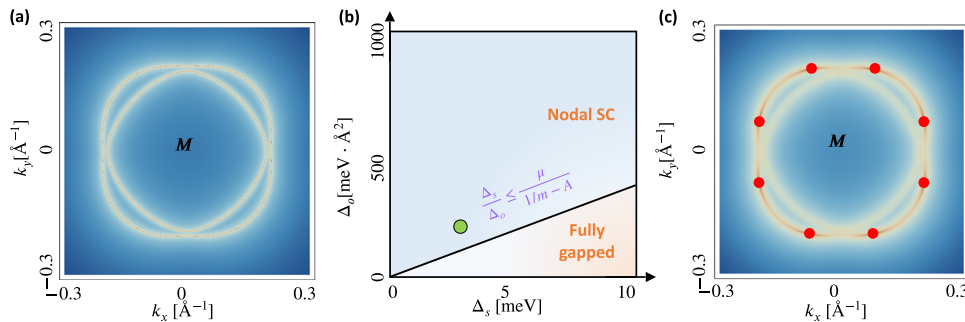
Fig. 2 The application to iron-chalcogenide superconductors with/without linear Dirac nodes. In (**a**), the two-electron pockets around the M point. For zero spin-orbit coupling, $v_{so} = 0$, (**b**) shows the phase diagram as a function of the intra-orbital pairing Δ_s and the inter-orbital pairing Δ_o. For the gap parameters represented by the green dot in (**b**), the nodal superconductor is exhibited in (**c**), where the eight dark red points represent the chiral symmetry-protected Dirac nodes.

induced nodal SC. In experiments, the nodal gap structure could be detected by measuring the temperature dependence of physical quantities like specific heat and penetration depth at low temperatures. A power law dependence usually indicates the existence of nodal structures (point nodes or line nodes), whereas exponential dependence implies the SC is fully gapped[3].

Applications to superconductors with nematic order. In addition to the crystal field splitting, the many-body electron-electron interactions may also lead to orbital hybridization, such as the nematic ordering in the normal states (See Supplementary Note 5 for details). The rotational symmetry reduction could either be from interaction-induced spontaneous symmetry breaking or from explicit symmetry breaking from, say, adding external strain. Then the natural question to ask is whether it is still possible to have an orbital-dependent pairing order characterized by some $\mathbf{d}_o$-vector? Interestingly, we find that the orbital-dependent pairing can coexist with the electronic nematic ordering as long as $\mathbf{d}_o$ is parallel to the $\mathbf{g}_{tot}$, which is an effective orbital-hybridization vector that also contains the nematic order. This establishes a deep connection between SCs with nematic order and spin-singlet orbital-triplet pairings. In the following, we study two typical examples.

- For case A [two-orbital system], we apply the theory to fit the anisotropic superconducting gap of the hole pocket in the bulk FeSe measured by the quasiparticle interference imaging[12].
- For case B [two-valley system], we use a toy model to demonstrate the possible existence of $s + d$-like nematic nodal superconductor in two-valley systems on a honeycomb lattice. We also show the transition between U-shaped and V-shaped quasi-particle density-of-state by tuning the chemical potential.

Case A: two-orbital model for the bulk FeSe SC. We discussed the possible anisotropic A_{1g}-type s-wave pairing states for the C_4-symmetric iron-chalcogenide SCs including fully gapped FeSe thin film and nodal SC in LiFeP and LaFePO. Here we investigate the C_4-breaking nematic SC in bulk FeSe. Let us revisit the iron-based SC with a well-established nematic ordering. We consider $\mathcal{H}_{int} = v_1 \hat{n}_1(\mathbf{r})\hat{n}_2(\mathbf{r})$, where $\hat{n}_i$ is electron density operator for the i-atomic orbital. If $\langle \hat{n}_1 \rangle \neq \langle \hat{n}_2 \rangle$, C_n ($n > 2$) is spontaneously broken down to C_2 and we have the nematic order. The intra-orbital interaction does not alter the mean-field results for nematic orders (See Supplementary Note 5). The total inter-orbital hybridization contains two parts,

$$\mathbf{g}_{tot}(\mathbf{k}) = \mathbf{g}_o(\mathbf{k}) + \mathbf{g}_{nem}, \qquad (17)$$

where $\mathbf{g}_o(\mathbf{k})$ is caused by the crystal field splitting and $\mathbf{g}_{nem} = (0, 0, \Phi)$ is induced due to the nematicity $\Phi = v_1 \langle \hat{n}_1 - \hat{n}_2 \rangle$, which is momentum-independent if translation symmetry is to be preserved. Hereafter, we focus on the hole pockets around the Γ point to fit the experimental data of superconducting gap functions[12]. We will see that even this simplified weak-coupling model, where the coupling between the hole pockets at the Γ point and the electron pockets at the M point is ignored, can produce a descent fit the experimental data. A similar result is expected for the electron pockets near the M point. Replacing $\mathbf{g}_o$ with $\mathbf{g}_{tot}$ in Eq. (5), we can still use Eq. (8) to investigate the interplay between superconductivity and nematic order, thus the orbital $\mathbf{d}_o$-vector satisfying $\mathbf{d}_o \| \mathbf{g}_{tot}$ leads to the nematic superconductivity. Thus, it generally shows the A_{1g}-type s-wave spin-singlet orbital-triplet pairings in nematic SCs.

This scenario can be adopted to study the quasi-two dimensional bulk FeSe, where superconductivity ($T_c \sim 8$ K) emerges inside a well-developed nematic phase (transition temperature $T_{nem} \sim 90$ K[36]), shown in Fig. 3a. For a minimal two-band model[37] for the bulk FeSe with $\{d_{xz}, d_{yz}\}$-orbitals, $\mathbf{g}_o = (2k_x k_y, 0, k_x^2 - k_y^2)$ and $\mathbf{g}_{nem} = (0, 0, \Phi)$[38,39]. Therefore, the nematic orbital $\mathbf{d}_o$-vector with $\mathbf{d}_o \| \mathbf{g}_{tot}$ breaks C_4 (see Supplementary Note 5 for more details). The projected pairing gap function on the large Fermi surface is given by

$$\Delta_{FS}(\mathbf{k}) = \Delta_s + \Delta_o \sqrt{\left(-\lambda_o(k_x^2 - k_y^2) + \Phi\right)^2 + (2\lambda_o k_x k_y)^2}. \qquad (18)$$

If $\Phi = 0$, $\Delta_{FS}(\mathbf{k})$ is reduced to $\Delta_s + \Delta_o |\lambda_o|(k_x^2 + k_y^2)$ that is in the isotropic limit. The presence of Φ is the driving force for the anisotropy of $\Delta_{FS}(\mathbf{k})$. When the nematicity Φ is strong enough, the orbital $\mathbf{d}_o$-vector will be pinned along the z-axis, resulting in the so-called orbital-selective pairing states. We adopt the realistic parameters for the bulk FeSe SC from Ref. 39 to calculate the superconducting gap measured by the quasiparticle interference imaging[12]. In Fig. 3b, we show the angular dependence of the pairing gap around the hole pocket at the Γ-point of FeSe in the presence of nematic order. Our theory provides an equally decent fit to recent experimental data[12] as the intra-orbital $s + d$-pairing theory proposed by Kang et al.[39], even though our work uses a simplified model without considering the coupling to the other two electron pockets. Our theory shows more clearly the role of nematic order on the pairing symmetries. Therefore, the theory developed in this work may alternatively explain the experimental evidence of orbital-selective pairings of the FeSe SC in refs. [12,27], and reveal a deep connection between nematic SC and spin-singlet orbital-triplet pairings. It has to be mentioned that here we only focused on the hole pockets around the Γ point and discussed the nematicity-induced gap anisotropy around the hole FS. There are other possible mechanisms for gap anisotropy in
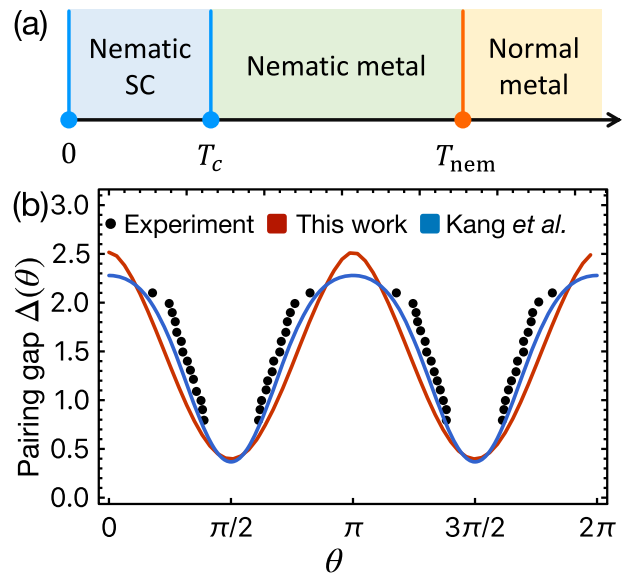
Fig. 3 The application to bulk FeSe superconductors with nematicity.
a Schematic phase diagram vs temperature T for normal metal ($T > T_{nem}$), nematic metal ($T < T_{nem}$), and nematic superconductivity ($T < T_c$).
b Angular dependence of the superconducting pairing gap: comparison between experiment data (black dots) by Sprau et al. ref.[12], our theory (red line) and the theory proposed by Kang et al.[39] (blue line). Fitting parameters used for our model: $\Delta_s = 2.6$, $\Delta_o = -0.055$ in Eq. (18). All the other parameters used are the same[39], including the chemical potential, effective mass, orbital hybridization, and nematic order.

Fe-based SCs. For example, a previous work[40] discussed, among other things, the anisotropy/isotropy of the SC gap around the electron pockets at the M point, where the degree of anisotropy depends on the J_1-J_2 magnetic frustration in the proposed five-orbital t-J_1-J_2 microscopic model.

Case B: two-valley system superconductivity. Similar to the two-orbital systems considered above, we discuss in this section superconductivity in two-valley systems, like single layer graphene SC[41] or transition metal dichalcogenide (TMD)[42], where the pairing can be between opposite valleys $K_\pm$. The spin-singlet pairing is merely characterized by the orbital $\mathbf{d}_o$-vector with $\Delta_s = 0$ in Eq. (2). For the single-particle Hamiltonian, the inter-valley hopping is naturally forbidden by translational symmetry, namely, $\lambda_o = 0$ in Eq. (5). Then, we consider the inter-valley scattering Hamiltonian,
$\mathcal{H}_{\text{int}} = \sum_{\mathbf{k},\mathbf{k}',\sigma} V(\mathbf{k} - \mathbf{k}') c^\dagger_{+,\sigma}(\mathbf{k}) c_{+,\sigma}(\mathbf{k}') c^\dagger_{-,\sigma}(\mathbf{k}') c_{-,\sigma}(\mathbf{k})$. It generates the inter-valley coupling $\mathbf{g}_{\text{int}}$ by defining the order parameter $\Phi(\mathbf{k}) = \sum_{\mathbf{k}',\sigma} V(\mathbf{k} - \mathbf{k}') \langle c_{+,\sigma}(\mathbf{k}') c^\dagger_{-,\sigma}(\mathbf{k}') \rangle$ that spontaneously breaks the translational symmetry,

$$\mathbf{g}_{\text{int}}(\mathbf{k}) = (g_{\text{int},1}(\mathbf{k}), g_{\text{int},2}(\mathbf{k}), 0), \qquad (19)$$

where $g_{\text{int},1}(\mathbf{k}) = \text{Re}[\Phi(\mathbf{k})]$ and $g_{\text{int},2}(\mathbf{k}) = -\text{Im}[\Phi(\mathbf{k})]$. In this case, TRS is $\mathcal{T} = i\tau_1\sigma_2\mathcal{K}$ and IS is $\mathcal{I} = \tau_1\sigma_0$. The $\mathbf{d}_o$-vector is manifested as $\mathbf{d}_o = (d_1(\mathbf{k}), id_2(\mathbf{k}), 0)$ with $d_1(\mathbf{k}) = d_1(-\mathbf{k})$ and $d_2(\mathbf{k}) = -d_2(-\mathbf{k})$. Both $d_1(\mathbf{k})$ and $d_2(\mathbf{k})$ are real to preserve TRS. As for the interaction-induced $\mathbf{g}_{\text{int}}$, $\mathcal{T}$ and $\mathcal{I}$ require $g_{\text{int},1}(\mathbf{k}) = g_{\text{int},1}(-\mathbf{k})$ and $g_{\text{int},2}(\mathbf{k}) = 0$. By symmetry, there are two general possibilities. One is $g_{\text{int},1}(\mathbf{k}) = 1$, so $C_3 \times \mathcal{I} = C_6$ is preserved, and it describes the charge-density-wave order[43,44]. The other one is $g_{\text{int},1}(\mathbf{k}) \in \{k_x k_y, k_x^2 - k_y^2\}$ that spontaneously breaks C_6 down to C_2, forming a nematic order. This is experimentally possible for the strain-induced Kekul'e distortion (i.e., $\sqrt{3} \times \sqrt{3}$ type).

We next discuss superconductivity in the presence of inter-valley couplings, by replacing the $\mathbf{g}_o$-vector in Eq. (5) with the interaction-induced $\mathbf{g}_{\text{int}}$. As a result, Eq. (8) is still applicable. It is

similar to a recent work[45] where the charge order coexists with a sublattice-selective non-unitary pairing state.

The nematic inter-valley coupling is represented as $g_{\text{int},1}(\mathbf{k}) = 1 + 2t_1 k_x k_y + t_2(k_x^2 - k_y^2)$, which requires that $\mathbf{d}_o(\mathbf{k}) = (1 + 2t_1 k_x k_y + t_2(k_x^2 - k_y^2), 0, 0)$ (see Supplementary Note 6). Here the normalization factor has been dropped without changing the essential physics. The system is fully gapped if the s-wave gap is dominant ($1 \gg \sqrt{t_1^2 + t_2^2}$), otherwise, it is a d-wave dominant nodal SC ($1 \ll \sqrt{t_1^2 + t_2^2}$).

As a concrete toy model, we look at superconductivity on a generic honeycomb lattice with two valleys $K_\pm$, with the Hamiltonian around the two valleys given by,

$$\mathcal{H}_0(\mathbf{k}) = \epsilon(\mathbf{k})\tau_0\sigma_0 + \alpha\left(k_x^3 - 3k_x k_y^2\right)\tau_3\sigma_0, \qquad (20)$$

where the two-valley basis used here is given by $\psi^\dagger_{\mathbf{k}} = (c^\dagger_{K_+,\uparrow}(\mathbf{k}), c^\dagger_{K_+,\downarrow}(\mathbf{k}), c^\dagger_{K_-,\uparrow}(\mathbf{k}), c^\dagger_{K_-,\downarrow}(\mathbf{k}))$ and $\epsilon(\mathbf{k})$ takes the same form as in Eq. (5). The parameter α determines the C_3 anisotropy of the continuum model around each valley. This Hamiltonian was used as an effective model[46] to study twisted bilayer graphene.

Including the inter-valley scattering effects, the one-band model is given by

$$\mathcal{H}(\mathbf{k}) = \epsilon(\mathbf{k})\tau_0\sigma_0 + \alpha\left(k_x^3 - 3k_x k_y^2\right)\tau_3\sigma_0 + \lambda_{\text{int}}[\mathbf{g}_{\text{int}}(\mathbf{k}) \cdot \boldsymbol{\tau}]\sigma_0,$$
$$(21)$$

where the λ_{int} determines the strength of the inter-valley scattering. In Fig. 4, we present representative numerical results for Eq. (21). Panels (a–c) illustrate Fermi surfaces with varying parameters, while panels (d–f) depict the corresponding quasi-particle density of states (DOS).

In the absence of inter-valley scattering ($\lambda_{\text{int}} = 0$), the Fermi surfaces (FSs) around the two $K_\pm$ valleys are plotted in Fig. 4a. As expected, with a fully symmetric s-wave pairing characterized by $\mathbf{d}_o = (1, 0, 0)$, a fully gapped or U-shaped quasi-particle density-
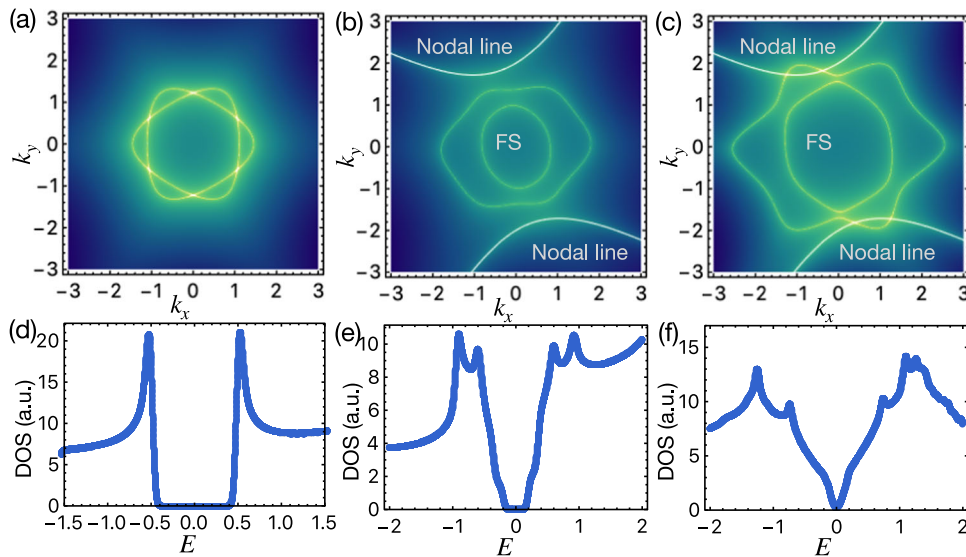
Fig. 4 Fermi surfaces (FSs) at the $K_\pm$ valleys and the quasi-particle density of states (DOS). Panels (**a–c**) show FSs with varying parameters, while panels (**d–f**) exhibit the corresponding quasi-particle DOS. The C_6 symmetric FS without inter-valley scattering is shown in (**a**) and its DOS with an isotropic s-wave pairing is given in (**d**). **b** Shows C_6-breaking FSs due to the inter-valley scattering, together with the nodal lines of nematic pairing. There are no nodes on the FSs and the corresponding DOS is shown in (**e**). **c** Is similar to (**b**) but with chemical potential μ adjusted so that the nodal lines intersect the FSs, hence a V-shaped DOS is obtained as in (**f**). Parameters used are the following, the C_3 anisotropy $\alpha = 0.2$, the coefficients for basis functions $t_1 = 0.15$, $t_2 = 0.25$, the orbital-dependent pairing gap $\Delta_o = 0.5$. For (**a**) and (**d**) $\mu = 1.5$ (chemical potential), the inter-valley coupling $g_{\text{int}} = 0$; for (**b**) and (**e**) $\mu = 1.5$, $g_{\text{int}} = 0.7$; for (**c**) and (**f**) $\mu = 2.7$, $g_{\text{int}} = 0.7$.

of-states (DOS) is obtained and shown in Fig. 4d. Then we include the aforementioned inter-valley scattering $\mathbf{g}_{int}$ that breaks C_6 down to C_2. As a result, our theory implies that the effective nematicity generated will favor a nematic pairing characterized by $\mathbf{d}_o \| \mathbf{g}_{int}$. Consider the generic form $\mathbf{d}_o = \mathbf{g}_{int} = (1 + 2t_1 k_x k_y + t_2(k_x^2 - k_y^2), 0, 0)$, the resulting C_6-breaking FS are shown in Fig. 4b, c, where the nodal lines of the pairing are also shown. By tuning the chemical potential μ, the FSs and nodal lines can go from non-intersecting in Fig. 4b to intersecting in Fig. 4c, leading to the corresponding evolution from the gapped U-shaped DOS in Fig. 4e to the gapless V-shaped DOS in Fig. 4f. Our results may explain the experimental observations in magic-angle twist bilayer graphene that reports the nematic order[47], and V-shaped DOS[48] at the specific doping level.

Discussions
We briefly discuss the difference between our theory and the previous studies[21] for nematic SCs. One example is a pairing state belonging to a 2D irreducible representation (Irrep), e.g., the E-pairing in Cu or Nb-doped Bi_2Se_3[49,50] and UPt_3[51,52]. A real order parameter vector $(\Delta_{E,1}, \Delta_{E,2})$ spontaneously breaks C_3, leading to nematic superconductivity. Alternatively, a nematic SC can be formed by mixing two different 1D-Irrep-pairing channels. In $FeSe$[53,54], the nematic order breaks the C_4 down to C_2, which mixes the s-wave and d-wave pairing channels. However, T_c of the $(s + d)$ orbital-independent pairing state could be generally affected by increasing nematicity, because of the significant change in the density of states at the Fermi energy. In our theory, the $(s + d)$-like nematic $\mathbf{d}_o$-vector coexists with the nematic order, so T_c is almost unaffected by increasing nematicity. Therefore, it may help to distinguish our results from previous proposals in experiments, where one may use the chemical or physical pressures to tune the nematicity and measure T_c as a function of

pressure[55]. Nevertheless, more efforts are necessary to test the results established in this work for nematic SCs.

In addition to the above discussions for the time-reversal-invariant superconducting states, we also comment on the effects of the spontaneous TRS-breaking, where a complex orbital $\mathbf{d}_o$-vector generates the orbital orderings as $\mathbf{M}_o = -i\gamma_1/\alpha_M(\mathbf{d} \times \mathbf{d}^*)$, of which only the y-component breaks TRS (see details in Supplementary Note 7), as illustrated in Fig. 5a. Alternatively, the corresponding quasi-particle spectrum in Fig. 5b shows the two distinct gaps, similar to the range given by Eq. (6). More explicitly, we schematically plot the atomic orbital-polarized density of states (DOS) by defining $|\pm\rangle = |1\rangle + i|2\rangle$ for complex orbitals, where $D_+ \neq D_-$ at finite energy clearly indicates that the DOS is orbital-polarized, which is consistent with the Ginzburg-Landau theory, shown in Supplementary Note 2. Moreover, we also find that the orbital-spin conversion would lead to the spin-polarized DOS[56].

The above result for orbital-triplet pairings is similar to the superconducting gaps for non-unitary spin-triplet SCs[3]. By symmetry, the Gizburg-Landau free energy is the same. To show the similarity, for the single-band spin-triplet SCs[57], the spin-triplet pairing potential is generally given by $\hat{\Delta}(\mathbf{k}) = \Delta_0[\mathbf{d}_s(\mathbf{k}) \cdot \boldsymbol{\sigma}](i\sigma_2)$, where Δ_0 is the pairing strength and $\boldsymbol{\sigma}$ are Pauli matrices in the spin subspace. Due to the Fermi statistics, the spin $\mathbf{d}_s(\mathbf{k})$-vector has to satisfy $\mathbf{d}_s(\mathbf{k}) = -\mathbf{d}_s(-\mathbf{k})$. The $\mathbf{d}_s$-vector formalism is firstly developed for He^3 superfluid[58]. And it also occurs in noncentrosymmetric SCs, the spin $\mathbf{d}_s(\mathbf{k})$-vector is usually pinned along a certain crystal axis since superconductivity is non-suppressed only for $\mathbf{d}_s(\mathbf{k}) \| \mathbf{g}_s(\mathbf{k})$, where $\mathbf{g}_s(\mathbf{k})$ represents the Rashba spin-orbit coupling (SOC)[4,6]. Besides, there is intrinsic spontaneous spin-polarization induced by the non-unitary pairing, $\mathbf{d}_s(\mathbf{k}) = k_z(1, -i\eta_0, 0)$ with real η_0. Fig. 5c shows the spin expectation value of the Cooper pairs ($\mathbf{M}_s \propto i\mathbf{d}_s^*(\mathbf{k}) \times \mathbf{d}_s(\mathbf{k}) = 2\eta_0 k_z^2 \vec{e}_z$). It is an equal-spin pairing so that σ_3 is conserved, and
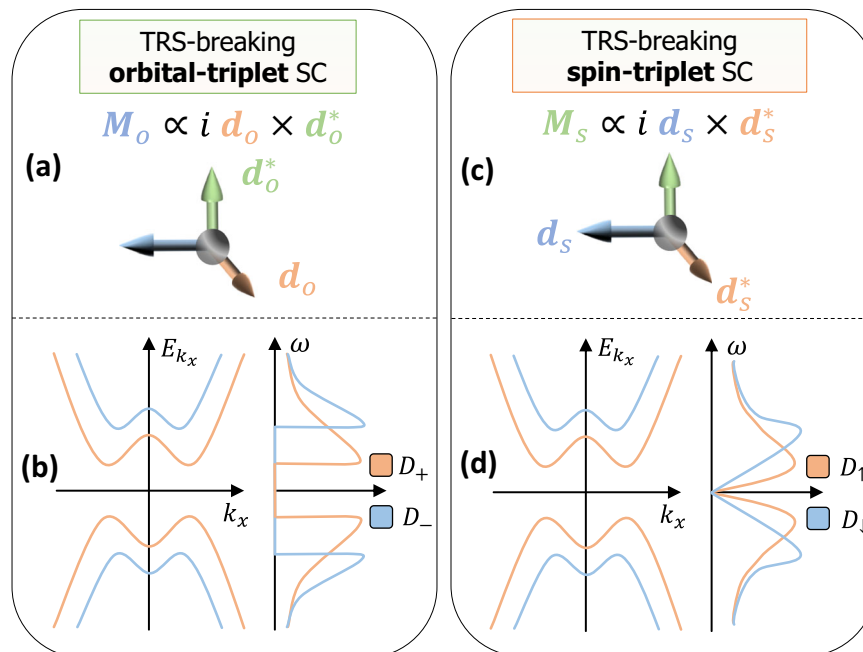
Fig. 5 Schematic diagrams for the time-reversal symmetry (TRS) breaking effects. a, b Are for orbital-triplet superconductors (SCs), while (**c**) and (**d**) are for spin-triplet SCs. As for orbital-triplet SCs characterized by a $\mathbf{d}_o$-vector, (**a**) shows a complex orbital $\mathbf{d}_o$-vector that spontaneously breaks TRS and results in the TRS-breaking orbital-polarization $\mathbf{M}_o \propto i\mathbf{d}_o \times \mathbf{d}_o^*$; and (**b**) shows the quasi-particle spectrum along k_x and the orbital-polarized density of states (DOS) $D_\pm$ with $|\pm\rangle$ representing $|1\rangle \pm i|2\rangle$. As a comparison, in spin-triplet SCs, (**c**) shows the superconductivity-induced spontaneous spin-polarization $\mathbf{M}_s \propto i\mathbf{d}_s \times \mathbf{d}_s^*$; and (**d**) shows the two distinct gaps of the quasi-particle spectrum along k_x and the spin-polarized DOS D_σ with $\sigma = \{\uparrow, \downarrow\}$. The gapped spectrum is plotted for $k_z \neq 0$ and the node in DOS profile is due to the nodal line at $k_z = 0$.

non-zero $\mathbf{M}_s$ leads to two distinct superconducting gaps of the quasi-particle spectrum[59], shown in Fig. 5d. In addition, the density of states (DOS) is spin-polarized, namely, $D_\uparrow \neq D_\downarrow$ at finite energy ω, as illustrated in Fig. 5d.

To summarize, we have derived a general weak-coupling criterion to investigate the spin-singlet orbital-triplet pairings in nematic SCs. For technical convenience, we adopt the orbital $\mathbf{d}_o$-vector to describe the spin-singlet orbital-dependent pairing states and the $\mathbf{g}_o$-vector for the orbital hybridizations. The main results of this work include, first, we demonstrate that an orbital $\mathbf{d}_o$-vector that is parallel with $\mathbf{g}_o$-vector for orbital hybridizations is possible to be realized in real superconducting materials. Second, the interplay between intra-orbital and orbital-dependent pairings that belong to the same symmetry representation can explain the observation of robust Dirac nodes in the quasi-2D iron-based SCs. Remarkably, we find that $\mathbf{d}_o$-vectors could even coexist with many-body interaction-induced nematic orders or charge-density-wave orders when $\mathbf{d}_o \propto \mathbf{g}_{tot} = \mathbf{g}_o + \mathbf{g}_{nem}$ (or $\mathbf{g}_{int}$). Moreover, our theory discovers the important role of nematic orders in SC pairing symmetry, which builds a possible bridge between repulsive interaction-induced nematic orders and nematic superconductivity and also reveals a deep connection between spin-singlet orbital-triplet pairings in nematic SCs. Our results may be helpful in understanding the nematic superconductivity in bulk FeSe. Our work will motivate more theoretical and experimental efforts to search for spin-singlet orbital-triplet SCs, even for topological superconductivity, which might contribute to further understanding the effects of spontaneous symmetry breaking on superconductivity.

Methods
Here we present the derivation for the main result Eq. (8), which is first order in λ_o, by solving the linearized gap equation. The second-order results are presented in Supplementary Note 3. The general $\mathbf{k} \cdot \mathbf{p}$ normal Hamiltonian considered in the main text reads,

$$\mathcal{H}_0(\mathbf{k}) = \epsilon(\mathbf{k})\tau_0\sigma_0 + \lambda_o(\mathbf{g}_o(\mathbf{k}) \cdot \boldsymbol{\tau})\sigma_0, \tag{22}$$

where the electronic basis is made of $\{1,2\}$-orbitals $\Psi_{\mathbf{k}}^\dagger = (c_{1,\uparrow}^\dagger(\mathbf{k}), c_{1,\downarrow}^\dagger(\mathbf{k}), c_{2,\uparrow}^\dagger(\mathbf{k}), c_{2,\downarrow}^\dagger(\mathbf{k}))$, $\epsilon(\mathbf{k}) = (k_x^2 + k_y^2)/2m - \mu$ is the band energy measured relative to the chemical potential μ, λ_o represents the orbital hybridization and $\mathbf{g}_o(\mathbf{k}) = (g_1, g_2, g_3(\mathbf{k}))$. The TRS $\mathcal{T} = i\sigma_2\tau_0\mathcal{K}$ requires $g_{1,3}(\mathbf{k}) = g_{1,3}(-\mathbf{k})$ and $g_2(\mathbf{k}) = -g_2(-\mathbf{k})$. It leads that

$$\mathbf{g}_o(\mathbf{k}) \cdot \boldsymbol{\tau} = [\mathbf{g}_o(-\mathbf{k}) \cdot \boldsymbol{\tau}]^*. \tag{23}$$

Besides, we set $\lambda_o > 0$ without loss of generality. The Matsubara Green's function for electrons is $G_e(\mathbf{k}, i\omega_n) = [i\omega_n - \mathcal{H}_0(\mathbf{k})]^{-1}$ and that for holes is $G_h(\mathbf{k}, i\omega_n) = -G_e^*(\mathbf{k}, i\omega_n)$. Here $\beta = 1/k_B T$ and $\omega_n = (2n+1)\pi/\beta$ with n integer. Therefore,

$$G_e(\mathbf{k}, i\omega_n) = \frac{\mathcal{P}_-(\mathbf{k})}{i\omega_n - \epsilon(\mathbf{k}) + \lambda_o|\mathbf{g}_o(\mathbf{k})|} + \frac{\mathcal{P}_+(\mathbf{k})}{i\omega_n - \epsilon(\mathbf{k}) - \lambda_o|\mathbf{g}_o(\mathbf{k})|}$$
$$\triangleq G_e^-(\mathbf{k}, i\omega_n)\mathcal{P}_-(\mathbf{k}) + G_e^+(\mathbf{k}, i\omega_n)\mathcal{P}_+(\mathbf{k}), \tag{24}$$

$$G_h(-\mathbf{k}, i\omega_n) = \frac{\mathcal{P}_-(\mathbf{k})}{i\omega_n + \epsilon(\mathbf{k}) - \lambda_o|\mathbf{g}_o(\mathbf{k})|} + \frac{\mathcal{P}_+(\mathbf{k})}{i\omega_n + \epsilon(\mathbf{k}) + \lambda_o|\mathbf{g}_o(\mathbf{k})|}$$
$$\triangleq G_h^-(\mathbf{k}, i\omega_n)\mathcal{P}_-(\mathbf{k}) + G_h^+(\mathbf{k}, i\omega_n)\mathcal{P}_+(\mathbf{k}), \tag{25}$$

where $\mathcal{P}_\pm(\mathbf{k}) = \frac{1}{2}(1 \pm \hat{\mathbf{g}}_o(\mathbf{k}) \cdot \boldsymbol{\tau})$ with $\hat{\mathbf{g}}_o(\mathbf{k}) = \mathbf{g}_o(\mathbf{k})/|\mathbf{g}_o(\mathbf{k})|$. Here $G_e^\pm(\mathbf{k}, i\omega_n) = \frac{1}{i\omega_n - \epsilon(\mathbf{k}) \mp \lambda_o|\mathbf{g}_o(\mathbf{k})|}$ and $G_h^\pm(\mathbf{k}, i\omega_n) = \frac{1}{i\omega_n + \epsilon(\mathbf{k}) \pm \lambda_o|\mathbf{g}_o(\mathbf{k})|}$. We expand the attractive interactions as

$$V_{s_1'a',s_2'b'}^{s_1a,s_2b}(\mathbf{k}, \mathbf{k}') = -\sum_{\Gamma,l} v_0^\Gamma [\mathbf{d}_o^{\Gamma,l}(\mathbf{k}) \cdot \boldsymbol{\tau} i\sigma_2]_{s_1a,s_2b}$$
$$\times [\mathbf{d}_o^{\Gamma,l}(\mathbf{k}') \cdot \boldsymbol{\tau} i\sigma_2]_{s_1'a',s_2'b'}, \tag{26}$$

where $v_0^\Gamma > 0$ is the interaction strength of the irreducible representation channel Γ of the crystalline group, and $l = 1, 2, ..., \text{Dim}\,\Gamma$. Each pairing channel Γ gives rise to an SC critical temperature T_c^Γ, and the actual transition temperature of the system is given by the largest of these critical temperatures. In our work, we mainly focus on the case where $\text{Dim}\,\Gamma = 1$, which is sufficient for the applications discussed in the main text. The coupling between orbital-dependent pairings and orbital-independent pairings will be discussed in detail later. The transition temperature T_c^Γ of orbital-dependent pairing channels is calculated by solving the linearized gap equation,

$$\Delta_{s_1,s_2}^{a,b}(\mathbf{k}) = -\frac{1}{\beta} \sum_{\omega_n} \sum_{s_1'a',s_2'b'} V_{s_1'a',s_2'b'}^{s_1a,s_2b}(\mathbf{k}, \mathbf{k}')$$
$$\times [G_e(\mathbf{k}', i\omega_n)\hat{\Delta}(\mathbf{k}')G_h(-\mathbf{k}', i\omega_n)]_{s_1'a',s_2'b'}, \tag{27}$$

which is reduced to $v_0^\Gamma \chi^\Gamma(T) - 1 = 0$ with the superconductivity susceptibility $\chi^\Gamma(T)$ in the channel Γ defined as,

$$\chi^\Gamma(T) = -\frac{1}{\beta}\sum_{\mathbf{k},\omega_n} \text{Tr}\left[(\mathbf{d}_o^\Gamma(\mathbf{k}) \cdot \boldsymbol{\tau} i\sigma_2)^\dagger G_e(\mathbf{k}, i\omega_n)(\mathbf{d}_o^\Gamma(\mathbf{k}) \cdot \boldsymbol{\tau} i\sigma_2)G_h(-\mathbf{k}, i\omega_n)\right], \tag{28}$$

$$= -\frac{2}{\beta}\sum_{\mathbf{k},\omega_n}\sum_{\alpha,\beta} G_e^\alpha(\mathbf{k}, i\omega_n)G_h^\beta(\mathbf{k}, i\omega_n)$$
$$\times \text{Tr}\left[(\mathbf{d}_o^\Gamma(\mathbf{k}) \cdot \boldsymbol{\tau})^\dagger \mathcal{P}_\alpha(\mathbf{k})(\mathbf{d}_o^\Gamma(\mathbf{k}) \cdot \boldsymbol{\tau})\mathcal{P}_\beta(\mathbf{k})\right], \tag{29}$$

where $\alpha, \beta \in \{+, -\}$. For notional simplicity, the superscript Γ will be dropped when there is no danger of confusion. Firstly, let us calculate the trace part. In the following calculation, we will use

$$\text{Tr}\left[(\mathbf{d}_o(\mathbf{k}) \cdot \boldsymbol{\tau})^\dagger \mathcal{P}_+(\mathbf{k})(\mathbf{d}_o(\mathbf{k}) \cdot \boldsymbol{\tau})\mathcal{P}_+(\mathbf{k})\right]$$
$$+ \text{Tr}\left[(\mathbf{d}_o(\mathbf{k}) \cdot \boldsymbol{\tau})^\dagger \mathcal{P}_-(\mathbf{k})(\mathbf{d}_o(\mathbf{k}) \cdot \boldsymbol{\tau})\mathcal{P}_-(\mathbf{k})\right]$$
$$= (\mathbf{d}_o^*(\mathbf{k}) \cdot \mathbf{d}_o(\mathbf{k})) + 2(\mathbf{d}_o^*(\mathbf{k}) \cdot \hat{\mathbf{g}}_o(\mathbf{k}))(\mathbf{d}_o(\mathbf{k}) \cdot \hat{\mathbf{g}}_o(\mathbf{k})) \tag{30}$$
$$- (\mathbf{d}_o^*(\mathbf{k}) \cdot \mathbf{d}_o(\mathbf{k}))(\hat{\mathbf{g}}_o(\mathbf{k}) \cdot \hat{\mathbf{g}}_o(\mathbf{k})).$$

And,

$$\text{Tr}\left[(\mathbf{d}_o(\mathbf{k}) \cdot \boldsymbol{\tau})^\dagger \mathcal{P}_+(\mathbf{k})(\mathbf{d}_o(\mathbf{k}) \cdot \boldsymbol{\tau})\mathcal{P}_-(\mathbf{k})\right]$$
$$+ \text{Tr}\left[(\mathbf{d}_o(\mathbf{k}) \cdot \boldsymbol{\tau})^\dagger \mathcal{P}_-(\mathbf{k})(\mathbf{d}_o(\mathbf{k}) \cdot \boldsymbol{\tau})\mathcal{P}_+(\mathbf{k})\right]$$
$$= (\mathbf{d}_o^*(\mathbf{k}) \cdot \mathbf{d}_o(\mathbf{k})) - 2(\mathbf{d}_o^*(\mathbf{k}) \cdot \hat{\mathbf{g}}_o(\mathbf{k}))(\mathbf{d}_o(\mathbf{k}) \cdot \hat{\mathbf{g}}_o(\mathbf{k})) \tag{31}$$
$$+ (\mathbf{d}_o^*(\mathbf{k}) \cdot \mathbf{d}_o(\mathbf{k}))(\hat{\mathbf{g}}_o(\mathbf{k}) \cdot \hat{\mathbf{g}}_o(\mathbf{k})).$$

Therefore, we arrive at

$$\text{Tr}\left[(\mathbf{d}_o(\mathbf{k}) \cdot \boldsymbol{\tau})^\dagger \mathcal{P}_\alpha(\mathbf{k})(\mathbf{d}_o(\mathbf{k}) \cdot \boldsymbol{\tau})\mathcal{P}_\beta(\mathbf{k})\right]$$
$$= \frac{1}{2}[(\mathbf{d}_o^*(\mathbf{k}) \cdot \mathbf{d}_o(\mathbf{k})) + i\alpha(\mathbf{d}_o(\mathbf{k}) \cdot (\mathbf{d}_o^*(\mathbf{k}) \times \hat{\mathbf{g}}_o(\mathbf{k})))$$
$$+ i\beta(\mathbf{d}_o^*(\mathbf{k}) \cdot (\mathbf{d}_o(\mathbf{k}) \times \hat{\mathbf{g}}_o(\mathbf{k}))) \tag{32}$$
$$+ \alpha\beta(2(\mathbf{d}_o^*(\mathbf{k}) \cdot \hat{\mathbf{g}}_o(\mathbf{k}))(\mathbf{d}_o(\mathbf{k}) \cdot \hat{\mathbf{g}}_o(\mathbf{k}))$$
$$- (\mathbf{d}_o^*(\mathbf{k}) \cdot \mathbf{d}_o(\mathbf{k}))(\hat{\mathbf{g}}_o(\mathbf{k}) \cdot \hat{\mathbf{g}}_o(\mathbf{k})))].$$

Then we have

$$\chi(T) = -\frac{1}{\beta} \sum_{\mathbf{k},\omega_n} \sum_{\alpha,\beta} G_e^\alpha(\mathbf{k}, i\omega_n) G_h^\beta(\mathbf{k}, i\omega_n)[(\mathbf{d}_o^*(\mathbf{k}) \cdot \mathbf{d}_o(\mathbf{k}))$$
$$+ i\alpha(\mathbf{d}_o(\mathbf{k}) \cdot (\mathbf{d}_o^*(\mathbf{k}) \times \hat{\mathbf{g}}_o(\mathbf{k}))) + i\beta(\mathbf{d}_o^*(\mathbf{k}) \cdot (\mathbf{d}_o(\mathbf{k}) \times \hat{\mathbf{g}}_o(\mathbf{k})))$$
$$+ \alpha\beta(2(\mathbf{d}_o^*(\mathbf{k}) \cdot \hat{\mathbf{g}}_o(\mathbf{k}))(\mathbf{d}_o(\mathbf{k}) \cdot \hat{\mathbf{g}}_o(\mathbf{k}))$$
$$- (\mathbf{d}_o^*(\mathbf{k}) \cdot \mathbf{d}_o(\mathbf{k}))(\hat{\mathbf{g}}_o(\mathbf{k}) \cdot \hat{\mathbf{g}}_o(\mathbf{k})))]. \tag{33}$$

Next, we calculate the integration for $\sum_{\mathbf{k},\omega_n}$ by using,

$$\sum_{\mathbf{k},\omega_n} \rightarrow \frac{N_0}{4} \int_{-\omega_D}^{+\omega_D} d\epsilon \int_S \frac{d\Omega}{2\pi} \sum_{\omega_n}, \tag{34}$$

where N_0 is the density of states at Fermi surface and Ω is the solid angle of $\mathbf{k}$ on Fermi surfaces. Then,

$$-\frac{N_0}{\beta} \int_{-\omega_D}^{+\omega_D} d\epsilon \int_S \frac{d\Omega}{2\pi} \sum_{\omega_n} G_e^+(\mathbf{k}, i\omega_n) G_h^+(\mathbf{k}, i\omega_n)$$
$$= -\frac{N_0}{\beta} \int_{-\omega_D}^{+\omega_D} d\epsilon \int_S \frac{d\Omega}{2\pi} \sum_{\omega_n} G_e^-(\mathbf{k}, i\omega_n) G_h^-(\mathbf{k}, i\omega_n) \tag{35}$$
$$\equiv \chi_0(T),$$

On one hand,

$$\int_{-\omega_D}^{+\omega_D} d\epsilon \sum_{\omega_n} G_e^+(\mathbf{k}, i\omega_n) G_h^+(\mathbf{k}, i\omega_n)$$
$$= \int_{-\omega_D}^{+\omega_D} d\epsilon \sum_{\omega_n} \frac{1}{i\omega_n + \epsilon} \frac{1}{i\omega_n - \epsilon} \tag{36}$$
$$= \beta \int_{-\omega_D}^{+\omega_D} d\epsilon \frac{\tanh\frac{\beta\epsilon}{2}}{2\epsilon}$$
$$= \beta \int_0^{\beta\omega_D/2} dx \frac{\tanh x}{x} \approx \beta \ln\left(\frac{2e^\gamma \omega_D}{\pi k_B T}\right),$$

where the approximation is done at low temperature when $\beta \rightarrow \infty$.

On the other hand, we could find a series representation for χ_0, which also applies to the case where $\lambda_o \neq 0$, so that $\chi_0 \equiv \chi(\lambda_o = 0)$ and $\chi(\lambda_o \neq 0)$ can be related by a simple relation. The way to do it is to perform the integration in ϵ first. More precisely,

$$\int_{-\omega_D}^{+\omega_D} d\epsilon \sum_{\omega_n} G_e^+(\mathbf{k}, i\omega_n) G_h^+(\mathbf{k}, i\omega_n)$$
$$= \int_{-\omega_D}^{+\omega_D} d\epsilon \sum_{\omega_n} \frac{1}{i\omega_n + \epsilon} \frac{1}{i\omega_n - \epsilon}$$
$$= 2\text{Re} \sum_{n \geq 0} \int_{-\omega_D}^{\omega_D} d\epsilon \frac{1}{i\omega_n + \epsilon} \frac{1}{i\omega_n - \epsilon} \tag{37}$$
$$= 2\beta\text{Re} \sum_{n \geq 0} \int_{-\beta\omega_D}^{\beta\omega_D} d\epsilon \frac{1}{i2\pi(n+1/2) + \epsilon} \frac{1}{i2\pi(n+1/2) - \epsilon}$$
$$\approx 2\beta\text{Re} \sum_{n \geq 0} \int_{-\infty}^{\infty} d\epsilon \frac{1}{i2\pi(n+1/2) + \epsilon} \frac{1}{i2\pi(n+1/2) - \epsilon}$$
$$= \beta\text{Re} \sum_{n \geq 0} \frac{1}{n+1/2},$$

where the low-temperature limit is again assumed and the integration is done using the residue theorem. In the same spirit, we have,

$$\int_{-\omega_D}^{+\omega_D} d\epsilon \sum_{\omega_n} G_e^+(\mathbf{k}, i\omega_n) G_h^-(\mathbf{k}, i\omega_n)$$
$$= \beta\text{Re} \sum_{n \geq 0} \frac{1}{n+1/2 + i\frac{\lambda_o|\mathbf{g}_o(\mathbf{k})|}{2\pi k_B T}}, \tag{38}$$

Now by introducing the digamma function defined on the complex plane,

$$\psi^{(0)}(z) = -\gamma + \sum_{n \geq 0}\left(\frac{1}{n+1} - \frac{1}{n+z}\right), \tag{39}$$

we have the following relation,

$$\int_{-\omega_D}^{+\omega_D} d\epsilon \sum_{\omega_n} G_e^+(\mathbf{k}, i\omega_n) G_h^-(\mathbf{k}, i\omega_n)$$
$$- \int_{-\omega_D}^{+\omega_D} d\epsilon \sum_{\omega_n} G_e^+(\mathbf{k}, i\omega_n) G_h^+(\mathbf{k}, i\omega_n)$$
$$= \beta \text{Re}\left[\psi^{(0)}\left(\frac{1}{2}\right) - \psi^{(0)}\left(\frac{1}{2} + i\frac{\lambda_o|\mathbf{g}(\mathbf{k})|}{2\pi k_B T}\right)\right] \tag{40}$$
$$\equiv \beta\mathcal{C}_0(T),$$

where $\chi_0(T) = N_0 \ln\left(\frac{2e^\gamma \omega_D}{\pi k_B T}\right)$, $\gamma = 0.57721\cdots$ is the Euler-Mascheroni constant and ω_D is the Debye frequency.

Therefore,

$$-\frac{N_0}{\beta} \int_{-\omega_D}^{+\omega_D} d\epsilon \int_S \frac{d\Omega}{2\pi} \sum_{\omega_n} G_e^-(\mathbf{k}, i\omega_n) G_h^+(\mathbf{k}, i\omega_n)$$
$$= -\frac{N_0}{\beta} \int_{-\omega_D}^{+\omega_D} d\epsilon \int_S \frac{d\Omega}{2\pi} \sum_{\omega_n} G_e^+(\mathbf{k}, i\omega_n) G_h^-(\mathbf{k}, i\omega_n) \tag{41}$$
$$= \chi_0(T) + N_0 \int_S \frac{d\Omega}{2\pi} \mathcal{C}_0(T).$$

Now we can proceed to calculate $\chi(T)$ given in Eq. (33),

$$\chi(T) = \chi_0(T) \int_S \frac{d\Omega}{2\pi} |\mathbf{d}_o \cdot \hat{\mathbf{g}}_o|^2 \tag{42}$$

$$+ \chi_0(T) \int_S \frac{d\Omega}{2\pi}\left(|\mathbf{d}_o|^2 - |\mathbf{d}_o \cdot \hat{\mathbf{g}}_o|^2\right) \tag{43}$$

$$+ N_0 \int_S \frac{d\Omega}{2\pi} \mathcal{C}_0(T)\left(|\mathbf{d}_o|^2 - |\mathbf{d}_o \cdot \hat{\mathbf{g}}_o|^2\right) \tag{44}$$

$$= \chi_0(T) + N_0 \int_S \frac{d\Omega}{2\pi} \mathcal{C}_0(T)\left(|\mathbf{d}_o|^2 - |\mathbf{d}_o \cdot \hat{\mathbf{g}}_o|^2\right). \tag{45}$$

In the calculation, we use normalized gap functions with $\int_S \frac{d\Omega}{2\pi} \mathbf{d}_o^* \cdot \mathbf{d}_o = 1$. It leads to,

$$\ln\left(\frac{T_c}{T_{c0}}\right) = \int_S \frac{d\Omega}{2\pi} \mathcal{C}_0(T_c)\left(|\mathbf{d}_o|^2 - |\mathbf{d}_o \cdot \hat{\mathbf{g}}_o|^2\right), \tag{46}$$

where T_{c0} is T_c for $\lambda_o = 0$ case by solving $v_0\chi_0(T_{c0}) = 1$. This is the Eq. (8) in the main text. In general, the right-hand side of Eq. (46) suppresses T_c. It clearly indicates that T_c would not be suppressed by orbital hybridization once $\mathbf{d}_o \| \mathbf{g}_o$ for all $\mathbf{k}$. So we conclude that the orbital $\mathbf{d}_o$-vector is possible to be stabilized in materials.

Data availability
The datasets generated during this study are available from the corresponding author upon reasonable request.

Code availability
The custom codes generated during this study are available from the corresponding author upon reasonable request.

References

1. Dresselhaus, M. S., Dresselhaus, G. & Jorio, A. *Group theory: application to the physics of condensed matter* (Springer Science & Business Media, 2007).
2. Chaikin, P. M., Lubensky, T. C. & Witten, T. A. *Principles of condensed matter physics*, vol. 10 (Cambridge university press Cambridge, 1995).
3. Sigrist, M. & Ueda, K. Phenomenological theory of unconventional superconductivity. *Rev. Mod. Phys.* **63**, 239–311 (1991).
4. Frigeri, P. A., Agterberg, D. F., Koga, A. & Sigrist, M. Superconductivity without inversion symmetry: Mnsi versus cept$_3$Si. *Phys. Rev. Lett.* **92**, 097001 (2004).
5. Fischer, M. H. Gap symmetry and stability analysis in the multi-orbital fe-based superconductors. *N. J. Phys.* **15**, 073006 (2013).
6. Ramires, A., Agterberg, D. F. & Sigrist, M. Tailoring T_c by symmetry principles: The concept of superconducting fitness. *Phys. Rev. B* **98**, 024501 (2018).
7. Andersen, L., Ramires, A., Wang, Z., Lorenz, T. & Ando, Y. Generalized anderson's theorem for superconductors derived from topological insulators. *Sci. Adv.* **6**, eaay6502 (2020).
8. Mackenzie, A. P. & Maeno, Y. The superconductivity of sr$_2$ruo$_4$ and the physics of spin-triplet pairing. *Rev. Mod. Phys.* **75**, 657–712 (2003).
9. Agterberg, D. F., Rice, T. M. & Sigrist, M. Orbital dependent superconductivity in sr$_2$ruo$_4$. *Phys. Rev. Lett.* **78**, 3374–3377 (1997).
10. Dai, X., Fang, Z., Zhou, Y. & Zhang, F.-C. Even parity, orbital singlet, and spin triplet pairing for superconducting lafeaso$_{1-x}$f$_x$. *Phys. Rev. Lett.* **101**, 057008 (2008).
11. Ong, T. T. & Coleman, P. Tetrahedral and orbital pairing: A fully gapped pairing scenario for the iron-based superconductors. *Phys. Rev. Lett.* **111**, 217003 (2013).
12. Sprau, P. O. et al. Discovery of orbital-selective cooper pairing in fese. *Science* **357**, 75–80 (2017).
13. Nica, E. M. & Si, Q. Multiorbital singlet pairing and d+ d superconductivity. *npj Quantum Mater.* **6**, 1–11 (2021).
14. Fu, L. & Berg, E. Odd-parity topological superconductors: Theory and application to cu$_x$bi$_2$se$_3$. *Phys. Rev. Lett.* **105**, 097001 (2010).
15. Brydon, P. M. R., Wang, L., Weinert, M. & Agterberg, D. F. Pairing of $j = 3/2$ fermions in half-heusler superconductors. *Phys. Rev. Lett.* **116**, 177001 (2016).
16. Yang, W., Li, Y. & Wu, C. Topological septet pairing with spin-$\frac{3}{2}$ fermions: High-partial-wave channel counterpart of the $^3He − b$ phase. *Phys. Rev. Lett.* **117**, 075301 (2016).
17. Savary, L., Ruhman, J., Venderbos, J. W. F., Fu, L. & Lee, P. A. Superconductivity in three-dimensional spin-orbit coupled semimetals. *Phys. Rev. B* **96**, 214514 (2017).
18. Yu, J. & Liu, C.-X. Singlet-quintet mixing in spin-orbit coupled superconductors with $j = \frac{3}{2}$ fermions. *Phys. Rev. B* **98**, 104514 (2018).
19. Scalapino, D. J. A common thread: The pairing interaction for unconventional superconductors. *Rev. Mod. Phys.* **84**, 1383–1417 (2012).
20. Fradkin, E., Kivelson, S. A., Lawler, M. J., Eisenstein, J. P. & Mackenzie, A. P. Nematic fermi fluids in condensed matter physics. *Annu. Rev. Condens. Matter Phys.* **1**, 153–178 (2010).
21. Fernandes, R. M., Orth, P. P. & Schmalian, J. Intertwined vestigial order in quantum materials: Nematicity and beyond. *Ann. Rev. Cond. Matter Phys.* **10**, 133–154 (2019).
22. Sigrist, M. Time-reversal symmetry breaking states in high-temperature superconductors. *Progr. Theor. Phys.* **99**, 899–929 (1998).
23. Lee, W.-C., Zhang, S.-C. & Wu, C. Pairing state with a time-reversal symmetry breaking in feas-based superconductors. *Phys. Rev. Lett.* **102**, 217002 (2009).
24. Hu, L.-H., Johnson, P. D. & Wu, C. Pairing symmetry and topological surface state in iron-chalcogenide superconductors. *Phys. Rev. Res.* **2**, 022021 (2020).
25. Lado, J. L. & Sigrist, M. Detecting nonunitary multiorbital superconductivity with dirac points at finite energies. *Phys. Rev. Res.* **1**, 033107 (2019).
26. Hu, L.-H., Wang, X. & Shang, T. Spontaneous magnetization in unitary superconductors with time reversal symmetry breaking. *Phys. Rev. B* **104**, 054520 (2021).
27. McQueen, T. M. et al. Tetragonal-to-orthorhombic structural phase transition at 90 k in the superconductor fe$_{1.01}$Se. *Phys. Rev. Lett.* **103**, 057002 (2009).
28. Ong, T., Coleman, P. & Schmalian, J. Concealed d-wave pairs in the s± condensate of iron-based superconductors. *Proc. Natl. Acad. Sci.* **113**, 5486–5491 (2016).
29. Agterberg, D. F., Shishidou, T., O'Halloran, J., Brydon, P. M. R. & Weinert, M. Resilient nodeless d-wave superconductivity in monolayer fese. *Phys. Rev. Lett.* **119**, 267001 (2017).
30. Smidman, M., Salamon, M. B., Yuan, H. Q. & Agterberg, D. F. Superconductivity and spin–orbit coupling in non-centrosymmetric materials: a review. *Reports on Progress in Physics* **80**, 036501 (2017).
31. Zhang, Y. et al. Superconducting gap anisotropy in monolayer fese thin film. *Phys. Rev. Lett.* **117**, 117001 (2016).
32. Fletcher, J. D. et al. Evidence for a nodal-line superconducting state in lafepo. *Phys. Rev. Lett.* **102**, 147001 (2009).
33. Hashimoto, K. et al. Nodal versus nodeless behaviors of the order parameters of lifep and lifeas superconductors from magnetic penetration-depth measurements. *Phys. Rev. Lett.* **108**, 047003 (2012).
34. Nakayama, T., Shishidou, T. & Agterberg, D. F. Nodal topology in d-wave superconducting monolayer fese. *Phys. Rev. B* **98**, 214503 (2018).
35. Eugenio, P. M. & Vafek, O. Classification of symmetry derived pairing at the m point in fese. *Phys. Rev. B* **98**, 014503 (2018).
36. Böhmer, A. E. & Kreisel, A. Nematicity, magnetism and superconductivity in fese. *Journal of Physics: Condensed Matter* **30**, 023001 (2017).
37. Raghu, S., Qi, X.-L., Liu, C.-X., Scalapino, D. J. & Zhang, S.-C. Minimal two-band model of the superconducting iron oxypnictides. *Phys. Rev. B* **77**, 220503 (2008).
38. Chubukov, A. V., Khodas, M. & Fernandes, R. M. Magnetism, superconductivity, and spontaneous orbital order in iron-based superconductors: Which comes first and why? *Phys. Rev. X* **6**, 041045 (2016).
39. Kang, J., Fernandes, R. M. & Chubukov, A. Superconductivity in fese: The role of nematic order. *Phys. Rev. Lett.* **120**, 267001 (2018).
40. Yu, R., Zhu, J.-X. & Si, Q. Orbital-selective superconductivity, gap anisotropy, and spin resonance excitations in a multiorbital t-J_1-J_2 model for iron pnictides. *Phys. Rev. B* **89**, 024509 (2014).
41. Wang, W.-S. et al. Functional renormalization group and variational monte carlo studies of the electronic instabilities in graphene near $\frac{1}{4}$ doping. *Phys. Rev. B* **85**, 035414 (2012).
42. Hsu, Y.-T., Vaezi, A., Fischer, M. H. & Kim, E.-A. Topological superconductivity in monolayer transition metal dichalcogenides. *Nat. Commun.* **8**, 14985 (2017).
43. Gutiérrez, C. et al. Imaging chiral symmetry breaking from kekulé bond order in graphene. *Nat. Phys.* **12**, 950–958 (2016).
44. Bao, C. et al. Experimental evidence of chiral symmetry breaking in kekulé-ordered graphene. *Phys. Rev. Lett.* **126**, 206804 (2021).
45. Wolf, T. M. R., Holst, M. F., Sigrist, M. & Lado, J. L. Nonunitary multiorbital superconductivity from competing interactions in dirac materials. *Phys. Rev. Res.* **4**, L012036 (2022).
46. You, Y.-Z. & Vishwanath, A. Superconductivity from valley fluctuations and approximate so (4) symmetry in a weak coupling theory of twisted bilayer graphene. *npj Quantum Mater.* **4**, 1–12 (2019).
47. Cao, Y. et al. Nematicity and competing orders in superconducting magic-angle graphene. *Science* **372**, 264–271 (2021).
48. Kim, H. et al. Spectroscopic signatures of strong correlations and unconventional superconductivity in twisted trilayer graphene. *arXiv e-prints* arXiv:2109.12127 (2021). 2109.12127.
49. Fu, L. Odd-parity topological superconductor with nematic order: Application to cu$_x$bi$_2$se$_3$. *Phys. Rev. B* **90**, 100509 (2014).
50. Matano, K., Kriener, M., Segawa, K., Ando, Y. & Zheng, G.-q Spin-rotation symmetry breaking in the superconducting state of cu$_x$bi$_2$se$_3$. *Nat. Phys.* **12**, 852–854 (2016).
51. Sauls, J. The order parameter for the superconducting phases of upt$_3$. *Adv. Phys.* **43**, 113–141 (1994).
52. Strand, J. et al. The transition between real and complex superconducting order parameter phases in upt3. *Science* **328**, 1368–1369 (2010).
53. Fernandes, R. M. & Millis, A. J. Nematicity as a probe of superconducting pairing in iron-based superconductors. *Phys. Rev. Lett.* **111**, 127001 (2013).
54. Kang, J., Kemper, A. F. & Fernandes, R. M. Manipulation of gap nodes by uniaxial strain in iron-based superconductors. *Phys. Rev. Lett.* **113**, 217001 (2014).
55. Matsuura, K. et al. Maximizing tc by tuning nematicity and magnetism in fese$_{1-x}$s$_x$ superconductors. *Nat. Commun.* **8**, 1–6 (2017).
56. Zeng, M., Xu, D.-H., Wang, Z.-M. & Hu, L.-H. Spin-orbit coupled superconductivity with spin-singlet nonunitary pairing. *Phys. Rev. B* **107**, 094507 (2023).
57. Leggett, A. J. A theoretical description of the new phases of liquid ^{3}He. *Rev. Mod. Phys.* **47**, 331–414 (1975).
58. Salomaa, M. M. & Volovik, G. E. Quantized vortices in superfluid ^{3}He. *Rev. Mod. Phys.* **59**, 533–613 (1987).
59. Sigrist, M. Introduction to unconventional superconductivity. In *AIP Conference Proceedings*, vol. 789, 165–243 (American Institute of Physics, 2005). https://doi.org/10.1063/1.2080350.

Author contributions

Competing interests

The authors declare no competing interests.

Additional information

Supplementary information The online version contains supplementary material available at https://doi.org/10.1038/s42005-023-01495-4.

Correspondence and requests for materials should be addressed to Lun-Hui Hu.

Peer review information *Communications Physics* thanks Yashar Komijani and the other, anonymous, reviewer(s) for their contribution to the peer review of this work. A peer review file is available.

Reprints and permission information is available at http://www.nature.com/reprints

Publisher's note Springer Nature remains neutral with regard to jurisdictional claims in published maps and institutional affiliations.